ARCHIVES OF ELECTRICAL ENGINEERING VOL. 68(1), pp. 195–208 (2019)

DOI 10.24425/aee.2019.125990

Numerical model of the axial magnetic bearing with six cylindrical poles

Barłomiej Marian Sikora, Adam Krzysztof Pilat

AGH University of Science and Technology, Poland
e-mail: {ap/bsikora}@agh.edu.pl

(Received: 04.10.2018, revised: 11.12.2018)

Abstract: The paper presents a numerical model of the novel design of the axial magnetic bearing with six cylindrical poles. The motivation behind this idea was to eliminate vibrations in rotating machinery due to the axial load. Common conception of such a bearing provides a single component of the electromagnetic force, which is not enough to reduce transverse and lateral vibrations of the armature. The proposed design allows for avoiding wobbling of the disc with the use of a few axial force components that are able to actively compensate the axial load and stabilise the disc in a balanced position. Before a real device is manufactured, a virtual prototype should be prepared. The accurate numerical model will provide essential knowledge about the performance of the axial magnetic bearing.

Key words: Active Magnetic Bearing, Axial Magnetic Bearing, Finite Element Method, numerical model, COMSOL Multiphysics

1. Introduction

Magnetic bearings use a magnetic levitation phenomenon, in order to obtain suspension of the rotor shaft, by producing the electromagnetic force without mechanical contact.

To provide a control of the rotating machine in the axial direction, the Axial Active Magnetic Bearings (AAMBs) are being widely used in space systems, physics, robotics and industrial applications [11]. The design of the Active Magnetic Bearings (AMBs) is in a constant evaluation, starting with a structure using permanent magnets [1, 3, 6, 9, 17], a typical active configuration, which contains two ring solenoid magnets [2, 18, 19], by inserting permanent magnets in the magnetic circuit [19, 20, 21], the use of separate pole pieces [8], up to a hybrid design, in which the function of an axial and radial bearing is combined [4, 7, 12, 22, 23]. In [5] a novel structure with a cylindrical rotor core was presented. However, this idea uses permanent magnets, which introduced an unbalanced force during displacement in a radial direction.

The design method and optimization procedure of the AMB were also examined in [10, 15, 16]. The magnetic circuit method was used, together with the Finite Element Method (FEM), in order to verify the feasibility of the proposed design. Although, it must be considered, that

when the magnetic circuit method is used, the nonlinearity of a material's B–H curve is not taken into account and some simplifications need to be introduced, such as a uniform distribution of the magnetic field in the bearing space. Moreover, the magnetic flux of the AMB's core remains in the unsaturated state and a leakage flux is neglected. In [13, 14] a dynamic model of the AMB, which was developed in COMSOL Multiphysics, is presented. Attention is paid to the investigation of particular components of the electromagnetic force. The completed research expands the knowledge related to the electromagnetic force.

2. Axial magnetic bearing model

The Axial Active Magnetic Bearing was designed to prevent motion of the shaft in the axial direction. In principle it has a feature to control disc tilting (Fig. 1(b)). The actuator, made of low-carbon steel S355JR and S235JR with the stator's thickness of 4 mm, consists of six poles in the form of pins, each with a height of 6 mm, placed circumferentially every 60° (Fig. 1(a)), with circular coils. The electromagnet is created by six coils, whose windings are placed around six poles. The set of parameters is given in Table 1. The coils can be connected in parallel or in series. In addition, they may be divided into groups, to introduce additional components of the axial force in case of tilt motion of the disc.

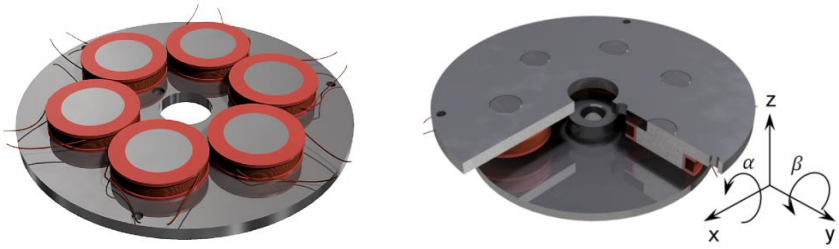

(a) (b)

Fig. 1. Model of the six pole Axial Active Magnetic Bearing (a) and its cross-section with proposed coordinate system (b)

Table 1. Parameters of the Axial Magnetic Bearing

Parameter	Description	Value
m	total mass of the disc	0.117 kg
z_0	nominal air gap	0.5 mm
N	number of coil turns of the single pole	50
R	cooper resistance of each pole	0.6 Ω
S	cross-section of the pole	254.5 mm^2
l	average path-length between poles in metal	77 mm
μ_r	relative permeability of steel S355JR	500

3. Numerical model with single electromagnet

In the designed in COMSOL Multiphysics and presented 3D models, the electromagnetic force was calculated, by using Maxwell's stress tensor integrated over the exterior surfaces of the selected armature domain. It is the most general method, however, it requires an air or vacuum domain around the armature, because the Maxwell stress tensor is defined on the material's boundary and distributed to the determined domain via its structure. This method is also very sensitive to mesh, which should be refined inside and symmetric around the calculated domain.

3.1. Titling motion of the disc with a single electromagnet

The first set of simulations concerns the tilting motion of the disc with only a single electromagnet of the AAMB, with the constant air gap z equal to 1 mm. The disc was rotated around its two orthogonal axis of the plane, which is perpendicular to the axial direction (see Fig. 1(b)). The rotation was determined by two angles: α and β, which vary from $-0.5°$ to $0.5°$.

A three-dimensional vector of the electromagnetic force was obtained (Figs. 2, 3).

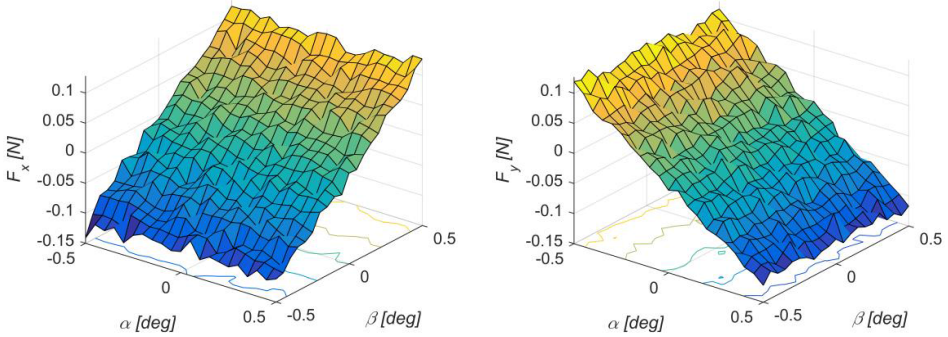

(a) (b)

Fig. 2. The x-component (a) and y-component (b) of the electromagnetic force F_z in the function of simulated disc tilting, for current $i = 2$ A and air gap $z = 1$ mm

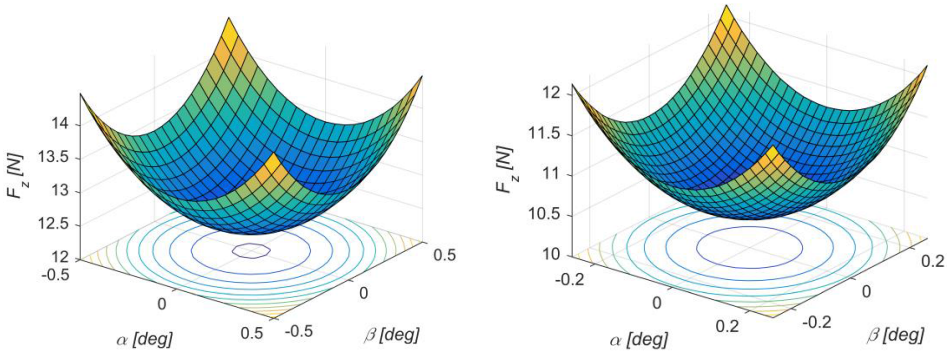

(a) (b)

Fig. 3. The axial component of the electromagnetic force F_z versus that of disc tilting: for current $i = 2$ A and air gap $z = 1$ mm (a); for current $i = 1$ A and air gap $z = 0.5$ mm (b)

3.2. Axial motion of the disc with a top electromagnet

In second set of simulations, the motion of the disc was axially constrained. The total air gap between the two AAMBs is 1 mm and the position of the disc in the middle of this distance corresponds to 0.5 mm (Fig. 4(a)).

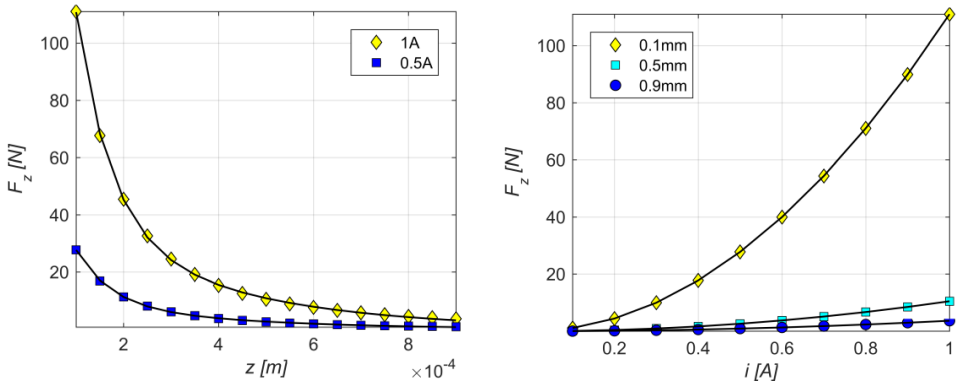

(a) (b)

Fig. 4. The axial component of the electromagnetic force F_z in the function of air gap z (a), in the function of current i (b)

One can find nonlinear characteristics of the electromagnetic force with respect to the coil current and disc displacement. Analysis of the achieved data allowed for proposing mathematical function (1) corresponding to a fixed coil current.

$$F_z(z) = a \cdot e^{b \cdot z} + c \cdot e^{d \cdot z}. \tag{1}$$

Table 2. Coefficients of approximation functions (Fig. 4(a)) for $i = 1$ A

Parameter	a	b	c	d
Value	−297.90	−13 750	−47.94	−3 021

The electromagnetic force versus the current (Fig. 4(b)) may be approximated by a second-order polynomial. The coefficients for a few disc displacements are presented in Table 3.

Table 3. Coefficients of approximation function (Fig. 4(b))

z **[mm]**	0.1	0.5	0.9
Coefficient $p \cdot i^2$	111	10.51	3.68

Finally, the electromagnetic force can be represented by an analitycal function (see Fig. 5(a)) expressed by the following formula:

$$F_z(z, i) = a \cdot e^{-b \cdot z} \cdot i^2. \tag{2}$$

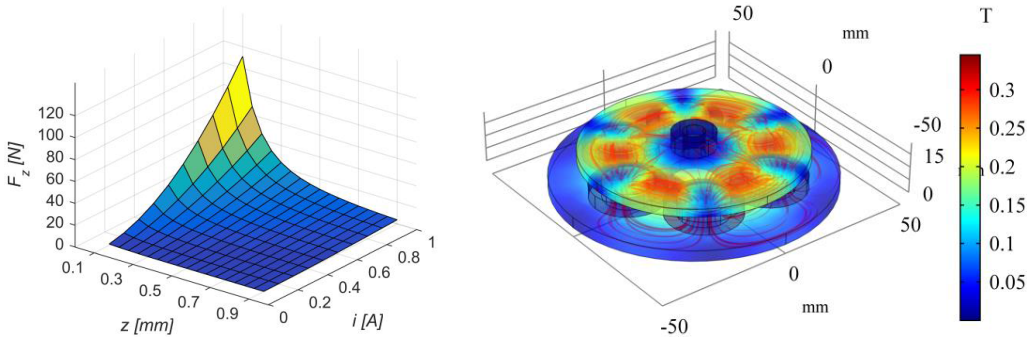

(a) (b)

Fig. 5. The electromagnetic force F_z in the function of air gap z and current i (a), the magnetic field distribution in the disc for $z = 500$ μm and $i = 1$ A ($B_{\max} = 0.3$ T)

Function (2) is monotonic. The goodness of fit is satisfying, the R-square error equals 0.98. The coefficients are presented in Table 4.

Table 4. Coefficients of approximation function (Fig. 5(a))

Parameter	a	b
Value	213.1	−7 117

The main parameters, which determine the behaviour of the armature in the magnetic levitation space, are the current k_i and displacement k_z stiffnesses (3). Both of them are crucial in the control system design procedure of the magnetic levitation systems (see Fig. 6(a), 6(b)). Fig. 6(c) presents the inductance L in relation to the displacement z. The function is described by Eq. (4).

$$k_i = \frac{\partial F_z}{\partial i}, \qquad k_z = \frac{\partial F_z}{\partial z}, \tag{3}$$

$$L(z) = a \cdot e^{\frac{-b}{z}} + c. \tag{4}$$

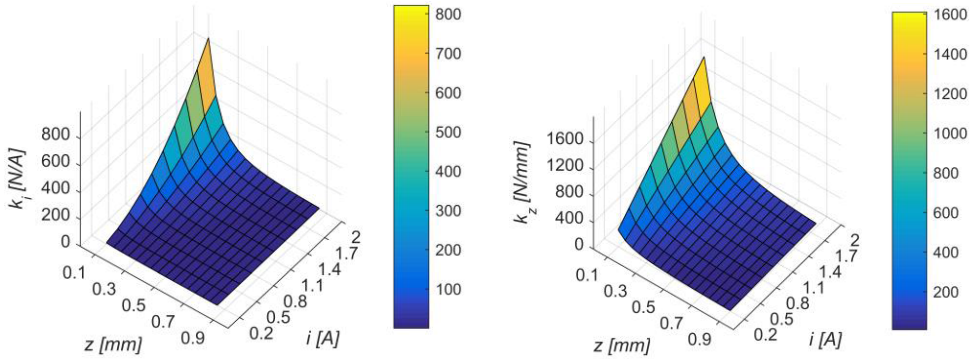

(a) (b)

Fig. 6.

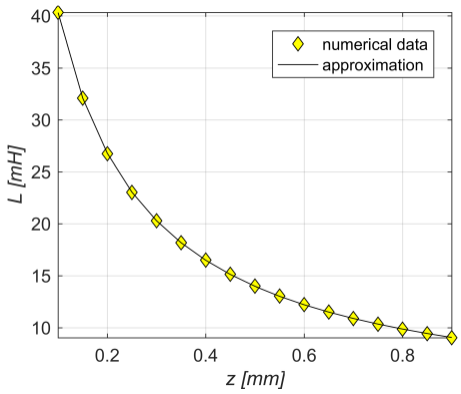

(c)

Fig. 6. The current (a) and displacement (b) stiffnesses k_i and k_z in the function of air gap z and current i; (c) the inductance L of the electromagnet in the function of air gap z

The R-square error of approximation (4) equals 0.99 and the coefficients are as follows:

$$a = -54.08, \quad b = 0.1207 \quad \text{and} \quad c = 56.42.$$

4. Numerical model with both electromagnets

4.1. Titling motion of the disc with top and bottom electromagnet

In this analysis, the zero value electromagnetic force is expected. However, due to the selected force calculation method, an outcome is sensitive to discretization of the levitation region. In the considered case, the geometrical dimensions of the magnetic bearing structure are significantly greater, relative to the air gap. This is often a cause of numerical errors (see Fig. 7).

In the case of both identical electromagnets, driven by the same current, with the disc located in the middle of the total air gap, all the forces should balance each other. Figs. 7(a) and 7(b) show the numerical noise, which varies from −0.05 N to 0.05 N for x and y component of the

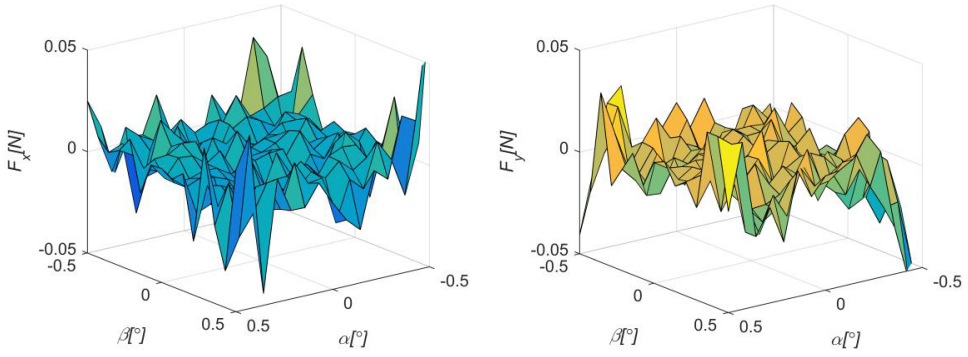

(a) (b)

Fig. 7.

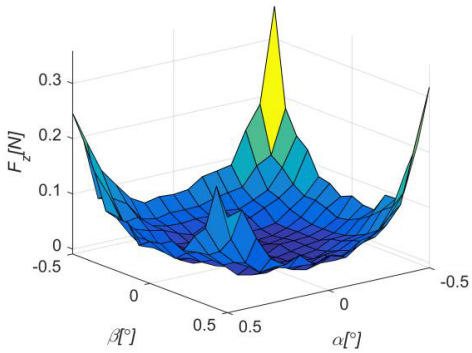

(c)

Fig. 7. The x (a), y (b) and axial-component (c) of the electromagnetic force F_z in the function of simulated disc tilting, for current $i = 1$ A and air gap $z = 0.5$ mm

force. In Fig. 7(c) numerical errors appear for large tilt angles. The reason is the decreasing air gap and non-adaptive mesh, which cause disturbed calculations and convergence difficulties. For a small air gap, the results are uncertain and simulation is time consuming.

Table 5 presents custom mesh settings. To improve convergence, linear discretization of the magnetic vector potential was selected. Conductivity of the air region was set to 0.1 S/m in order to avoid singularity error. The magnetic bearing geometry was surrounded by air sphere with radius of 75 mm.

Table 5. Mesh settings

Parameter	**Value**
maximum element size	8.25 mm
minimum element size	0.08 mm
curvature factor	0.4
resolution of narrow regions	0.7
maximum element growth rate	1.4
number of mesh elements	379 412

4.2. Axial motion of the disc with top and bottom electromagnet

The retrieved data is well approximated by function (5) for the fixed disc position with the parameters listed in Table 6.

$$F_z(i) = p_1 \cdot i^2 + p_2 \,. \tag{5}$$

Table 6. Coefficients of approximation functions (Fig. 9)

Parameter	a	b	c	d	p_1	p_2
0.5 A	0.0069	9 106	−62.16	−9 089	18 700	−9.37
1 A	0.02773	9 106	−248.6	−9 089	74 790	−37.49

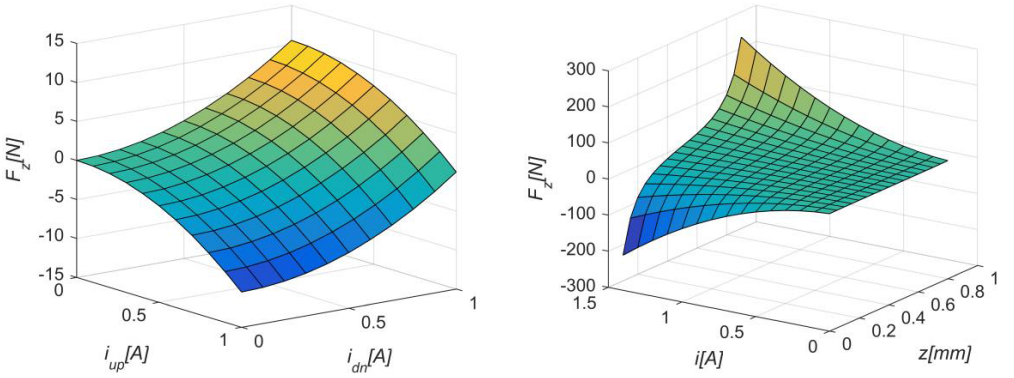

(a) (b)

Fig. 8. The axial component of the electromagnetic force F_z versus currents of bottom i_{dn} and top i_{up} electromagnet, for air gap $z = 0.5$ mm (a); versus air gap z and current i identical for both electromagnets (b)

The axial electromagnetic force (Fig. 9) may be approximated, by using functions (1 and 5). The coefficients are presented in Table 6.

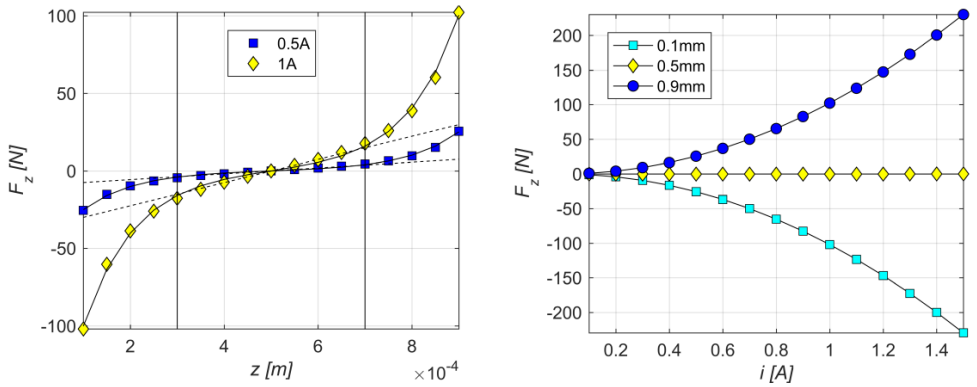

(a) (b)

Fig. 9. The axial component of the electromagnetic force F_z versus air gap z (a) versus current i (b), where current i is identical for both electromagnets

In the subsequent simulation, the bottom electromagnet was powered by a bias current of 0.5 A and the top electromagnet was driven by sum of a bias current and a load current, which varies from 0 to 1 A. Calculations were conducted for a variable disc location in the air gap (see Fig. 10(a)). Setting the bias current determines the linearity range of the force (see Fig. 10(b)).

Fig. 10(b) shows, that linearity range of the electromagnetic force is moved towards the bottom electromagnet and decreases, in comparison with Fig. 9(a). Nonlinearity of the force, hard upon the top electromagnet, occurs for larger values of the load current. Also the range of a linear characteristic is slighter (see Fig. 10(b)). For the load current equal to 1 A, it is from 2.5 mm to 5.5 mm.

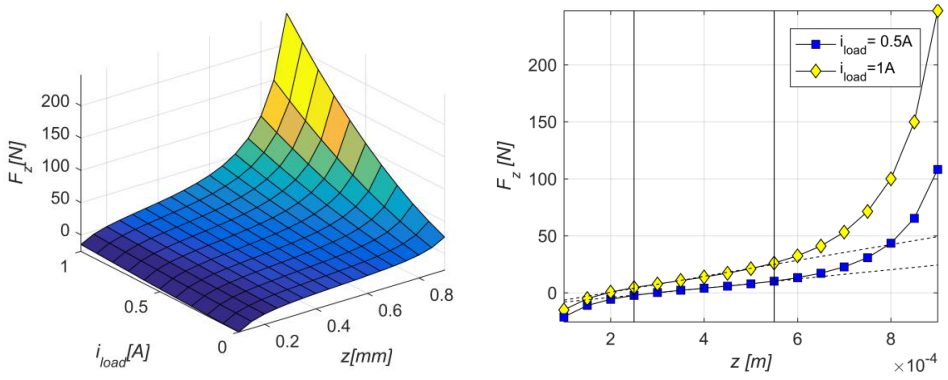

(a) (b)

Fig. 10. The axial component of the electromagnetic force F_z in the function of air gap z and load current (a) versus air gap z (b), for bias current equals to 0.5 A

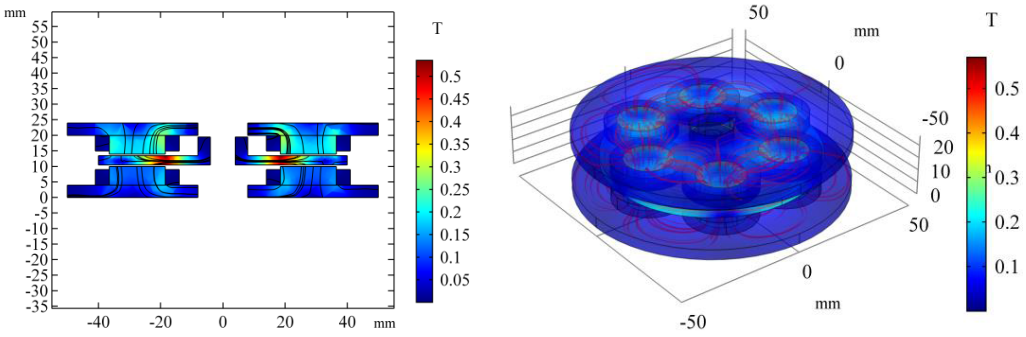

(a) (b)

Fig. 11. Magnetic field distribution for air gap $z = 0.5$ mm and current of the bottom and top electromagnet, respectively, 1 A bias and 1.5 A (a); 3D magnetic field distribution and its streamlines for the Axial Active Magnetic Bearing (b)

5. Eddy currents calculation

Finally, eddy currents were calculated due to the solid form of the electromagnet poles and the armature. Three simulation scenarios were chosen, to observe the consequences of increased frequency. Typically, the AMB operates at a constant current level, with a change corresponding to the time reaction due to axial motion of the rotor. In fact, there is no oscillatory motion, rather motion with damping characteristics. But let's assume, that a coil current will be harmonic and with frequencies, as follows: 10 Hz, 100 Hz, 1 000 Hz.

Having a numerical model, it is possible to analyse eddy currents induced in the pole. Fig. 13 shows the distribution of the eddy currents on poles' surface. One can find a tendency of growth and concentration of eddy currents on the outer edges of the poles, with respect to the increasing frequency.

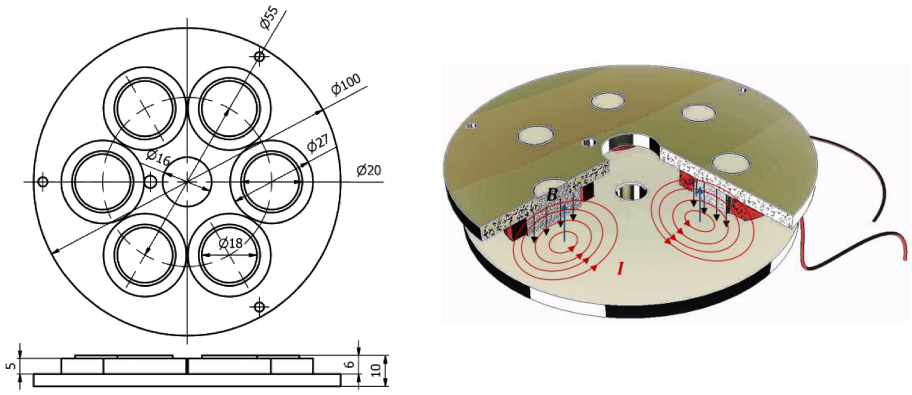

(a) (b)

Fig. 12. Detailed geometry of the considered Axial Active Magnetic Bearing (a); illustration of eddy currents (b)

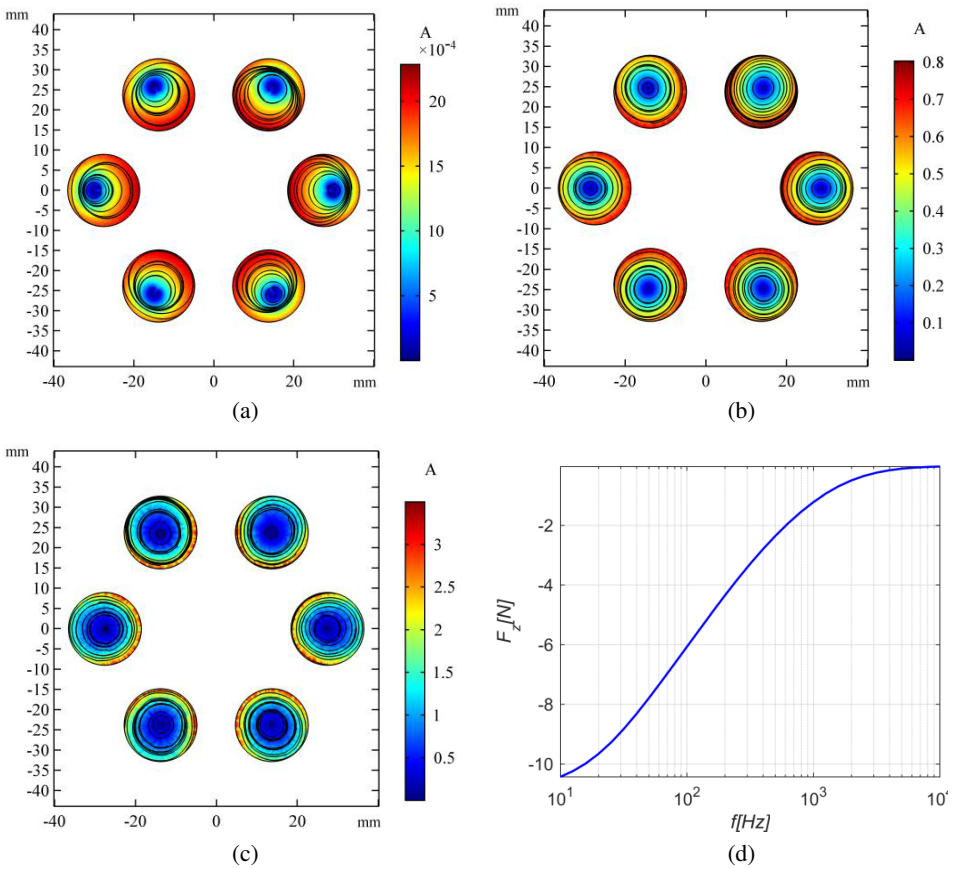

(a) (b) (c) (d)

Fig. 13. Eddy currents on poles' surface for frequency f 10 Hz (a); 100 Hz (b); 1 000 Hz (c) and the axial electromagnetic force F_z versus frequency in logarithmic scale (d)

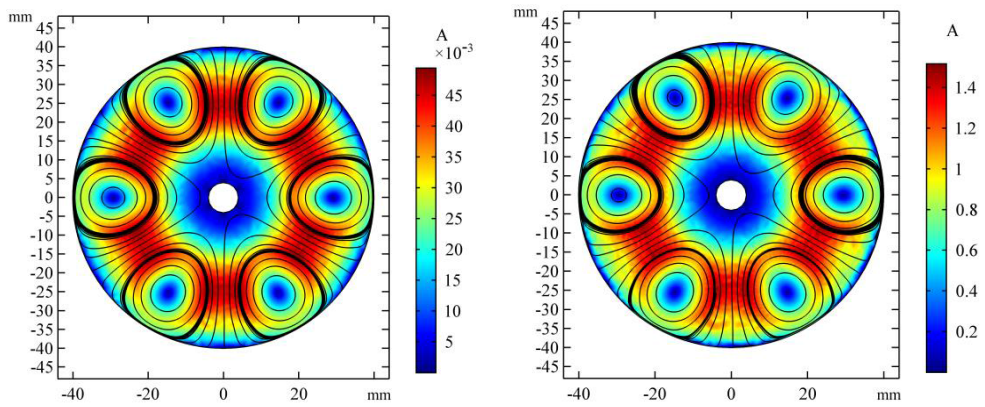

Fig. 14. Eddy currents on disc's surface for frequency f 10 Hz (a), 100 Hz (b)

At the end, the developed numerical model of the AAMB was examined with respect to the tilting simulation. The disc was rotated at specified values of angles α and β (see Fig. 1(b)). From the simulation results, presented in Fig. 15, we can read, that the magnetic flux density is changing with respect to the disc orientation. The parallel disc location, with respect to the AMB poles and magnetic flux distribution with marked poles, is presented in Fig. 15(a). One can analyse the control configuration of the cylinder electromagnets. When the disc is tilted, the magnetic flux density reflects the disc orientation. The practical application of this solution is the sensing feature of the proposed configuration. The values of the magnetic flux density are presented in details in Table 7. The examined configuration operates in a relatively small values of the magnetic flux density, therefore the nonlinear aspects will be considered in the future research.

Table 7. Magnetic flux density B_z on poles' surfaces: average, maximum and minimum values for poles 1, 2, 3 (see Fig. 15(a) for numbering)

α	β	**avg [T]**			**max [T]**			**min [T]**		
		B_{z1}	B_{z2}	B_{z3}	B_{z1}	B_{z2}	B_{z3}	B_{z1}	B_{z2}	B_{z3}
−0.5°	−0.5°	−0.115	0.086	−0.092	−0.077	0.140	−0.063	−0.187	0.058	−0.151
−0.5°	0	−0.098	0.098	−0.134	−0.070	0.151	−0.093	−0.149	0.069	−0.205
−0.5°	0.5°	−0.086	0.115	−0.234	−0.060	0.183	−0.146	−0.140	0.078	−0.405
0	−0.5°	−0.168	0.109	−0.094	−0.119	0.167	−0.068	−0.242	0.075	−0.151
0	0	−0.131	0.131	−0.131	−0.105	0.179	−0.104	−0.177	0.104	−0.182
0	0.5°	−0.109	0.168	−0.216	−0.075	0.248	−0.160	−0.170	0.117	−0.342
0.5°	−0.5°	−0.291	0.165	−0.092	−0.172	0.257	−0.064	−0.617	0.104	−0.151
0.5°	0	−0.202	0.202	−0.134	−0.145	0.295	−0.093	−0.293	0.153	−0.200
0.5°	0.5°	−0.165	0.291	−0.234	−0.113	0.645	−0.150	−0.254	0.179	−0.414

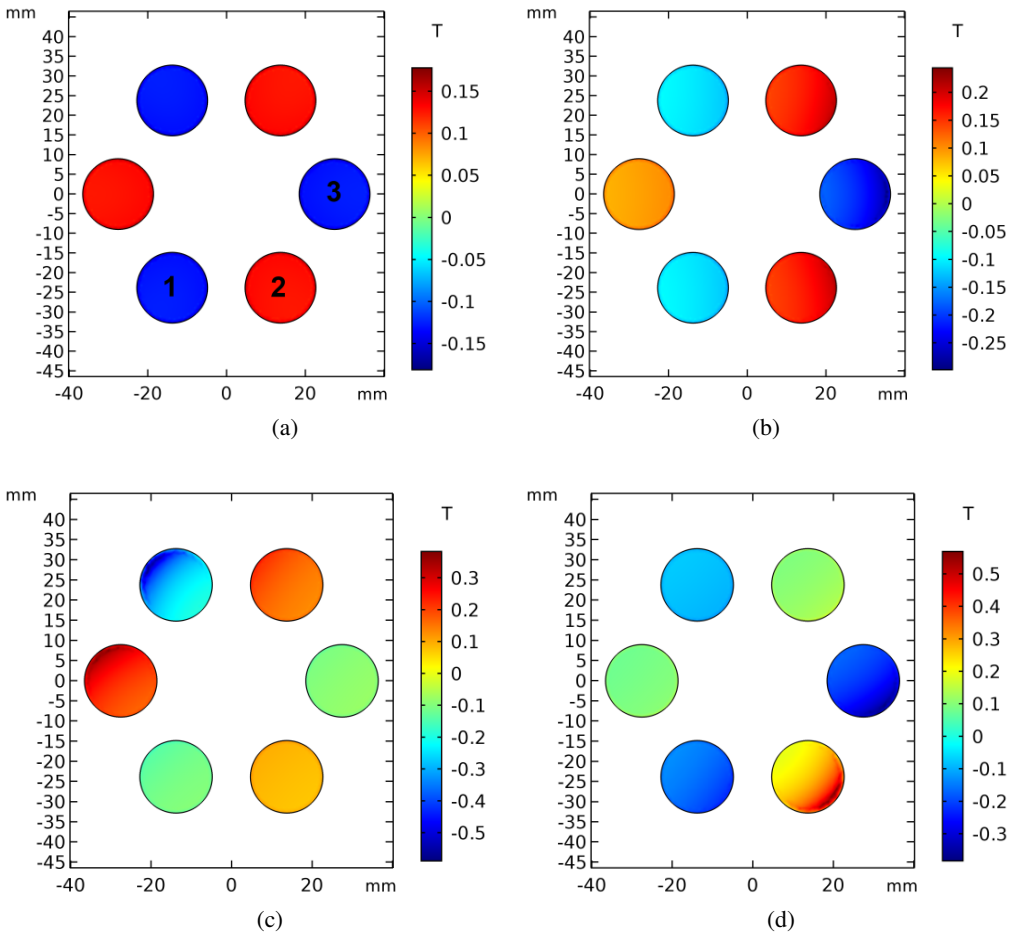

Fig. 15. Axial component of the magnetic flux density B_z on poles' surface, for different angles α and β of disc's rotation: $0°,\ 0°$ (a); $0°,\ 0.5°$ (b); $-0.5°,\ -0.5°$ (c); $0.5°,\ 0.5°$ (d)

During the modelling procedure of the electromagnetic actuator, a magnetic saturation should be taken into account. The saturation will occur especially in thinner ferromagnetic elements. Limits of induced magnetism in an armature must be investigated. The shape, size and configuration of the electromagnet will influence on application's practical limitations.

6. Conclusions

The conducted analysis, based on the Finite Element Method, provides a better insight into the phenomena observed in the AAMB. The description of the disc's motion in the bearing space plays a significant role during the design procedure. Based on FEM simulations, it is possible to

optimize the geometry of the actuator and the energy consumption of the proposed system. Also, prediction of the electromagnetic force value may be done, which is the main factor of the bearing stiffness. The electromagnetic force will be essential, when it comes to the controller design and operating range of the AAMB.

Acknowledgement

This work was supported by the Akademickie Centrum Komputerowe Cyfronet AGH as a part of calculation grant ActRotCtrl.

References

[1] Bachovchin D.K., Hoburg J.F., Post R.F., *Stable Levitation of a Passive Magnetic Bearing*, IEEE Transactions on Magnetics, vol. 49, no. 1, pp. 609–617 (2013).

[2] Barbaraci G., *Axial active magnetic bearing design*, Journal of Vibration and Control, vol. 22, iss. 5, pp. 1190–1197 (2014), DOI: 10.1177/1077546314534720.

[3] Burcan J., Slawinska A., *Self-controllable passive axial magnetic bearing*, Tribologia, no. 4, pp. 81–98 (2003).

[4] Han B., Liu X., Zheng S., *A Novel Integral 5-DOFs Hybrid Magnetic Bearing with One Permanent Magnet Ring Used for Turboexpander*, Mathematical Problems in Engineering, vol. 2014, no. 162561, pp. 1–18 (2014), DOI: 10.1155/2014/162561.

[5] Hijikata K. *et al.*, *Basic Characteristics of an Active Thrust Magnetic Bearing With a Cylindrical Rotor Core*, IEEE Transactions on Magnetics (2008).

[6] Horikawa O., da Silva I., *Single axis controlled attraction type magnetic bearing*, Journal of the Brazilian Society of Mechanical Sciences, ISSN 0100-7386, vol. 24, no. 4 (2002), DOI: 10.1590/S0100-73862002000400012.

[7] Imoberdorf P., Nussbaumer T., Kolar J.W., *Analysis of a combined radial-axial magnetic bearing for a high-speed drive system*, 5th IET International Conference on Power Electronics, Machines and Drives (PEMD 2010), Brighton, UK, pp. 1–6 (2010), DOI: 10.1049/cp.2010.0091.

[8] Ishino Y., Mizuno T., Takasaki M., Hara M., Yamaguchi D., *Development of a Compact Axial Active Magnetic Bearing with a Function of Two-Tilt-Motion Control*, Actuators, vol. 6, no. 2, p. 14 (2017), DOI: 10.3390/act6020014.

[9] Jinji S., Yuan R., Jiancheng F., *Passive axial magnetic bearing with Halbach magnetized array in magnetically suspended control moment gyro application*, Journal of Magnetism and Magnetic Materials, ISSN 0304-8853, vol. 323, iss. 15 (2011), pp. 2103–2107, DOI: 10.1016/j.jmmm.2011.02.020.

[10] Lv H. *et al.*, *Structure design and optimization of thrust magnetic bearing for the high-speed motor*, IEEE International Conference on Mechatronics and Automation (ICMA) (2017).

[11] Maslen E. *et al.*, *Magnetic Bearing Design for a High Speed Rotor*, Springer Berlin Heidelberg, Berlin (1989).

[12] McMullen P.T., Huynh C.S., Hayes R.J., *Combination Radial-Axial Magnetic Bearing*, Seventh International Symposium on Magnetic Bearings, ETH Zurich (2000).

[13] Pilat A., *A synergistic dynamic 2D FEM model of an active magnetic bearing with three electromagnets*, Diffusion and Defect Data – Solid State Data. Part B, Solid State Phenomena, SELM'2013: International Symposium on Electrodynamic and Mechatronic Systems, ISSN 1012-0394, vol. 214, pp. 106–112 (2014).

[14] Piłat A., *Analytical modeling of active magnetic bearing geometry*, Applied Mathematical Modelling, ISSN 0307-904X, vol. 34, no. 12, pp. 3805–3816 (2010).

[15] Pilat A., Sikora B., *Design and initial study of porous core electromagnet for levitation applications*, MSM 2018, 14th international conference Mechatronic Systems and Materials, AIP Conference Proceedings, ISSN 0094-243X, vol. 2029, iss. 1, Zakopane, Poland (2018).

[16] Pilat A., Sikora B., Klocek J., Cieślik J., *Set-up of active magnetic bearings for control of flexible shaft*, MSM 2018, 14th international conference Mechatronic Systems and Materials, AIP Conference Proceedings, ISSN 0094-243X, vol. 2029, iss. 1, Zakopane, Poland (2018).

[17] Ravaud R., Lemarquand G., *Halbach Structures for Permanent Magnet Bearings*, Progress in Electromagnetics Research M, vol. 14, pp. 236–277 (2010).

[18] Schweitzer G., *Magnetic Bearings*, Springer-Verlag, Zurich (1988).

[19] Schweitzer G., Maslen E.H., *Magnetic Bearings: Theory, Design and Application to Rotating Machinery*, Springer, Zurich (2009).

[20] Sikora B., Pilat A., *Hybrid Axial Active Magnetic Bearing – design, modelling and prototype*, International Symposium on Magnetic Bearings, Beijing, China (2018).

[21] Wajenrt D., Tomczuk B., *Simulation for the determination of the hybrid magnetic bearing's electromagnetic parameters*, Przeglad Elektrotechniczny, ISSN 0033-2097, R. 93 no. 2, pp. 157–160 (2017).

[22] Watkins J., Brown G., Blumenstock K., *Control of integrated radial and axial magnetic bearings*, Proceedings of the 33rd South Eastern Symposium on System Theory, Athens, OH, USA, pp. 1–5 (2001), DOI: 10.1109/SSST.2001.918480.

[23] Weißbacher C., Stelzer H., Hameyer K., *Application of a Tubular Linear Actuator as an Axial Magnetic Bearing*, IEEE/ASME Transactions on Mechatronics, vol. 15, no. 4, pp. 615-622 (2010).